

The ${}^6\text{H}$ states studied in the $d({}^8\text{He}, \alpha)$ reaction and evidence of extremely correlated character of the ${}^5\text{H}$ ground state

E.Yu. Nikolskii^{a,b,*}, I.A. Muzalevskii^{b,c}, A.A. Bezbakh^{b,c}, V. Chudoba^{b,c}, S.A. Krupko^b, S.G. Belogurov^{b,d}, D. Biare^b, A.S. Fomichev^{b,e}, E.M. Gazeeva^b, A.V. Gorshkov^b, L.V. Grigorenko^{b,d,a}, G. Kaminski^{b,f}, M.S. Khirk^{b,g}, O. Kiselev^h, D.A. Kostyleva^{h,i}, M.Yu. Kozlov^j, B. Mauryey^{b,k}, I. Mukha^h, W. Piatek^{b,f}, A.M. Quynh^{b,l}, V.N. Schetinin^j, A. Serikov^b, S.I. Sidorchuk^b, P.G. Sharov^{b,c}, N.B. Shulgina^{a,m}, R.S. Slepnev^b, S.V. Stepantsov^b, A. Swiercz^{b,n}, P. Szymkiewicz^{b,n}, G.M. Ter-Akopian^{b,e}, R. Wolski^{b,o}, B. Zalewski^{b,f}, M.V. Zhukov^p

^aNational Research Centre “Kurchatov Institute”, Kurchatov sq. 1, 123182 Moscow, Russia

^bTerov Laboratory of Nuclear Reactions, JINR, 141980 Dubna, Russia

^cInstitute of Physics, Silesian University in Opava, 74601 Opava, Czech Republic

^dNational Research Nuclear University “MEPhI”, 115409 Moscow, Russia

^eDubna State University, 141982 Dubna, Russia

^fHeavy Ion Laboratory, University of Warsaw, 02-093 Warsaw, Poland

^gFaculty of Physics, Moscow State University, 119991 Moscow, Russia

^hGESI Helmholtzzentrum für Schwerionenforschung GmbH, 64291 Darmstadt, Germany

ⁱII. Physikalisches Institut, Justus-Liebig-Universität, 35392 Giessen, Germany

^jLaboratory of Information Technologies, JINR, 141980 Dubna, Russia

^kInstitute of Nuclear Physics, 050032 Almaty, Kazakhstan

^lNuclear Research Institute, 670000 Dalat, Vietnam

^mBogoliubov Laboratory of Theoretical Physics, JINR, 141980 Dubna, Russia

ⁿAGH University of Science and Technology, Faculty of Physics and Applied Computer Science, 30-059 Krakow, Poland

^oInstitute of Nuclear Physics PAN, Radzikowskiego 152, 31342 Kraków, Poland

^pDepartment of Physics, Chalmers University of Technology, S-41296 Göteborg, Sweden

ABSTRACT

The extremely neutron-rich system ${}^6\text{H}$ was studied in the direct ${}^2\text{H}({}^8\text{He}, {}^4\text{He}){}^6\text{H}$ transfer reaction with a 26 A MeV secondary ${}^8\text{He}$ beam. The measured missing mass spectrum shows a resonant state in ${}^6\text{H}$ at 6.8(3) MeV relative to the ${}^3\text{H}+3n$ threshold. The population cross section of the presumably p -wave states in the energy range from 4 to 8 MeV is $d\sigma/d\Omega_{\text{c.m.}} \simeq 190(40) \mu\text{b/sr}$ in the angular range $5^\circ < \theta_{\text{c.m.}} < 16^\circ$. The obtained missing mass spectrum is free of the ${}^6\text{H}$ events below 3.5 MeV ($d\sigma/d\Omega_{\text{c.m.}} \lesssim 3 \mu\text{b/sr}$ in the same angular range). The steep rise of the ${}^6\text{H}$ missing mass spectrum at 3 MeV allows to show that 4.5(3) MeV is the lower limit for the possible resonant state energy in ${}^6\text{H}$ tolerated by our data. According to paring energy estimates, such a 4.5(3) MeV resonance is a realistic candidate for the ${}^6\text{H}$ ground state (g.s.). The obtained results confirm that the decay mechanism of the ${}^7\text{H}$ g.s. (located at 2.2 MeV above the ${}^3\text{H}+4n$ threshold) is the “true” (or simultaneous) $4n$ emission. The resonance energy profiles and the momentum distributions of the sequential ${}^6\text{H} \rightarrow {}^5\text{H}(\text{g.s.})+n \rightarrow {}^3\text{H}+3n$ decay fragments were analyzed by the theoretically-updated direct four-body-decay and sequential-emission mechanisms. The measured momentum distributions of the ${}^3\text{H}$ fragments in the ${}^6\text{H}$ rest frame indicate very strong “dineutron-type” correlations in the ${}^5\text{H}$ ground state decay.

Keywords: ${}^8\text{He}$ beam; deuteron transfer; three-neutron emission.

Date: June 15, 2021.

1. Introduction

One of the important trends of the modern experimental nuclear physics, taking advantages of the radioactive ion beam techniques, is the expansion of our knowledge on nuclear sys-

tems located further beyond the proton and neutron driplines. An important motivation here is the quest for the limits of existence of nuclear structure: how far should we go beyond the driplines before coming to situation when resonant structures become completely “dissolved in continuum”?

Recently, reliable spectroscopic information was obtained

*Corresponding author. E-mail address: enikolskii@mail.ru (E.Yu. Nikolskii)

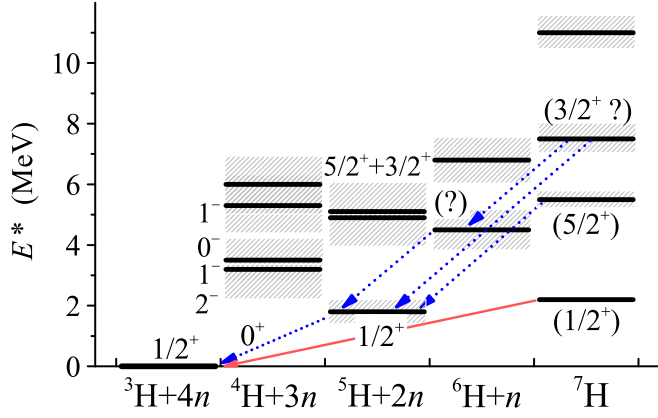


Fig. 1. The level schemes of ${}^6\text{H}$, and the known neighboring ${}^4\text{H}$, ${}^5\text{H}$ [8, 9, 10], and ${}^7\text{H}$ [1, 11] systems important for the discussions of this work. The solid red arrow illustrates the decay mechanism of ${}^7\text{H}$ g.s. which is expected to be “true” $4n$ emission. The dotted blue arrows illustrate the decay mechanism of the higher excitations in ${}^7\text{H}$, which is expected to be the sequential $2n+2n$ and $2n+n+n$ emissions via the ${}^5\text{H}$ and ${}^6\text{H}$ excited states, respectively.

on the extreme neutron-rich system ${}^7\text{H}$ produced in the ${}^2\text{He}({}^8\text{He}, {}^3\text{He}){}^7\text{H}$ reaction [1, 2, 3]. The ${}^6\text{H}$ population in the ${}^2\text{He}({}^8\text{He}, {}^4\text{He}){}^6\text{H}$ reaction, making the subject of the present work, is a natural “satellite” channel for the aforementioned experiment.

Experimental information on the ${}^6\text{H}$ resonant states is very limited. The authors of Ref. [4] reported a value $E_T = 2.7(4)$ MeV (energy above the ${}^3\text{H}+3n$ decay threshold) for the ${}^6\text{H}$ state produced in the ${}^7\text{Li}({}^7\text{Li}, {}^8\text{B}){}^6\text{H}$ reaction. A bit later this result was confirmed (with some reservations) in the ${}^9\text{Be}({}^{11}\text{B}, {}^{14}\text{O}){}^6\text{H}$ reaction [5], giving ${}^6\text{H}$ ground-state resonance at energy $E_T = 2.6(5)$ MeV. The observation of the ${}^6\text{H}$ resonant states at $E_T = \{6.6(7), 10.7(7), 15.3(7), 21.3(4)\}$ MeV, populated in the ${}^9\text{Be}(\pi^-, pd){}^6\text{H}$ reaction, was reported in Ref. [6]. The ${}^6\text{H}$ g.s. energy $E_T = 2.9(9)$ MeV was determined in the ${}^8\text{He}({}^{12}\text{C}, {}^6\text{H}){}^{14}\text{N}$ reaction [7]. The latter result, however, is not an independent one, since it is based on the two assumptions: (i) the 5 observed events spread from 0 to 7.5 MeV excitation in the MM spectrum of ${}^6\text{H}$ all really belong to ${}^6\text{H}$ (there was no channel identification in [7], which can distinguish among ${}^5\text{H}$, ${}^6\text{H}$, and ${}^7\text{H}$) and (ii) these events represent the resonant state consistent with those found in [4, 5]. Our results are in contradiction with [4, 5, 7].

The search for the ${}^6\text{H}$ resonant states is an exciting challenge in itself, however, here we face two important questions related also to our understanding of the neighboring systems.

(i) What are the decay mechanisms of the ${}^7\text{H}$ ground (~ 2.2 MeV) and excited (~ 5.5 MeV) states? This is defined by the spectra of its subsystems, see Fig. 1. For example, it could be either the true ${}^7\text{H} \rightarrow {}^3\text{H}+4n$ decay, or sequential ${}^7\text{H} \rightarrow {}^5\text{H}(\text{g.s.})+2n$, or, else, the ${}^7\text{H} \rightarrow {}^6\text{H}(\text{g.s.})+n$ decay, depending on the ground state energies of ${}^5\text{H}$ and ${}^6\text{H}$. While for ${}^4\text{H}$ and ${}^5\text{H}$ there are some relatively modern data, the spectrum of ${}^6\text{H}$ is too uncertain.

(ii) What is the decay mechanism of the ${}^6\text{H}$ ground state? Intuitive vision of the situation, also confirmed by the theoretical estimates of this work, tell us that the ${}^6\text{H}$ g.s. decay is likely to have a sequential ${}^6\text{H} \rightarrow {}^5\text{H}(\text{g.s.})+n \rightarrow {}^3\text{H}+3n$ character. In such a situation, by studying the ${}^6\text{H}$ decay, we also gain access to the decay properties of the ${}^5\text{H}$ ground state. The momentum distributions of the ${}^3\text{H}$ fragment, measured

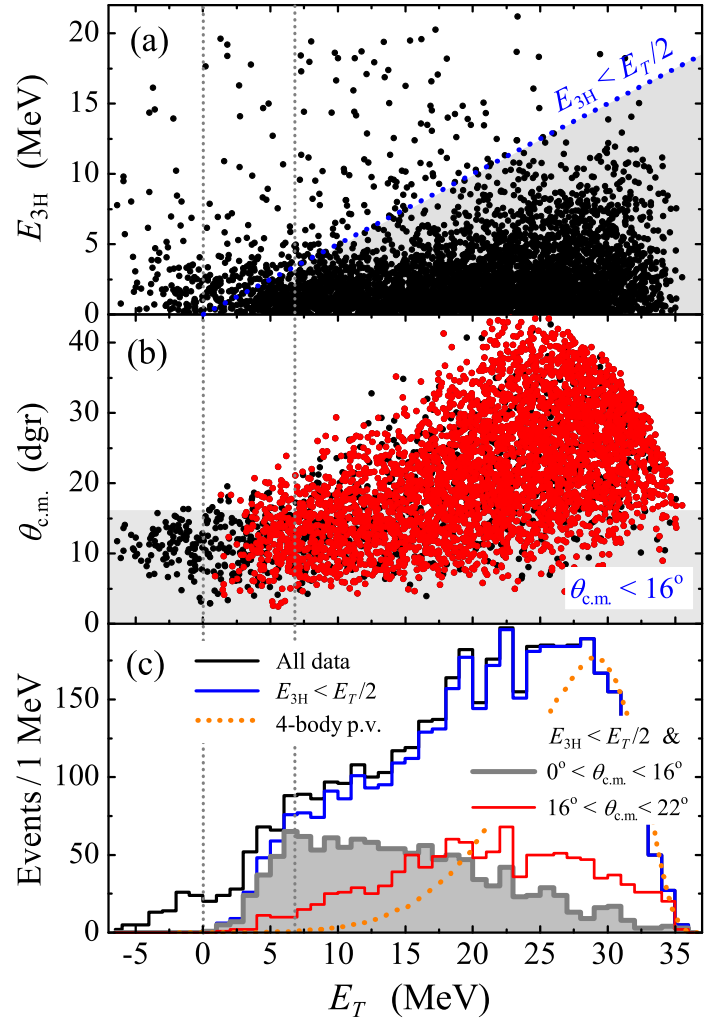


Fig. 2. Data on the ${}^4\text{He}$ - ${}^3\text{H}$ coincidence events considered for the ascertainment of the ${}^6\text{H}$ MM energy spectrum. (a) Correlation between the ${}^3\text{H}$ energy in the ${}^6\text{H}$ c.m. frame $E_{3\text{H}}$ and the ${}^6\text{H}$ MM energy E_T . The gray triangle, bounded by the blue dotted line, shows the kinematically allowed region. (b) Correlation between the center-of-mass reaction angle and the ${}^6\text{H}$ MM energy. The gray rectangle shows the $\theta_{\text{c.m.}} < 16^\circ$ cut-off region. (c) The ${}^6\text{H}$ missing mass: complete data (black histogram), kinematical cutoff $E_{3\text{H}} < E_T/2$ (blue histogram), and additional cutoff $\theta_{\text{c.m.}} < 16^\circ$ (filled gray histogram) and $16^\circ < \theta_{\text{c.m.}} < 22^\circ$ (red histogram). The orange dotted curve illustrates the 4-body phase volume $\sim E_T^{7/2}$ convoluted with the setup bias. The vertical gray dotted lines indicate the ${}^3\text{H}+3n$ threshold and the position of the 6.8 MeV ${}^6\text{H}$ resonant state.

in our experiment, can be interpreted by assuming an unexpectedly strong “dineutron” correlation character of the ${}^5\text{H}$ ground state decay. The sequential ${}^6\text{H} \rightarrow {}^5\text{H}(\text{g.s.})+n \rightarrow {}^3\text{H}+3n$ decay has never been studied before, and our results highlight the potential of such studies as an important source of information about the intermediate ${}^5\text{H}$ system.

The detailed information on the low-energy spectrum of ${}^6\text{H}$, obtained in this work shed light on the mentioned problems.

2. Experiment

The experiment was performed in the Flerov Laboratory of Nuclear Reactions (JINR, Dubna) at the ACCULINNA-2 fragment-separator recently coupled to the U-400M heavy ion cyclotron [12]. The study of ${}^6\text{H}$ was a “satellite” activity for experiments [1, 2] dedicated to ${}^7\text{H}$. The experiments were discussed in detail in Ref. [2], and we only briefly sketch here

the basic experimental information.

The ${}^6\text{H}$ system was produced in the ${}^2\text{H}({}^8\text{He}, {}^4\text{He}){}^6\text{H}$ reaction as a result of interaction of the secondary ${}^8\text{He}$ beam ($\sim 10^5$ pps at 26 A MeV energy and $\sim 90\%$ purity) with the deuterium nuclei in the cryogenic gas target of $3.7 \times 10^{20} \text{ cm}^{-2}$. The experimental setup involved 4 “sideway” telescopes, the “central” telescope, and the neutron wall. An assembly of four identical ΔE - E - E telescopes provided the detection of the ${}^4\text{He}$ recoil nuclei emitted in the angular range $\sim 8^\circ - 26^\circ$ in laboratory system. The 20 μm thick, $50 \times 50 \text{ mm}^2$ front single-side Si detector of the telescope had 16 strips. Next to this ΔE detector was the 1 mm thick, $61 \times 61 \text{ mm}^2$ double-side strip Si detector having behind another 1 mm thick veto detector. The central telescope, assigned for the registration of the ${}^3\text{H}$ fragments, originating from the ${}^6\text{H}$ decay, consisted of the 1.5 mm thick double sided Si strip detector followed by the 4×4 array of CsI(Tl) scintillators. The “fast” decay tritons ($E \sim 70 \pm 30 \text{ MeV}$), emitted in the narrow forward cone $\theta \leq 6^\circ$, were detected with good angular ($\Delta\theta \leq 0.5^\circ$) and energy ($\Delta E/E \leq 2\%$) resolutions. The setup also included a neutron wall of 48 stilbene-crystal modules [13] located near zero angle at a distance of $\sim 2 \text{ m}$ from the deuterium target. According to the Monte-Carlo (MC) simulations of the experimental setup, the typical efficiencies (at $E_T \sim 5 \text{ MeV}$) of double ${}^4\text{He}$ - ${}^3\text{H}$ and triple ${}^4\text{He}$ - ${}^3\text{H}$ - n coincidences were $\sim 65\%$ and $\sim 4\%$, respectively. The ${}^6\text{H}$ missing mass (MM) resolution was $\sim 1.7 \text{ MeV}$ and $\sim 1.4 \text{ MeV}$ FWHM at $E_T \sim 5 \text{ MeV}$ and $E_T \sim 10 \text{ MeV}$, respectively.

3. The ${}^6\text{H}$ data

The ${}^4\text{He}$ - ${}^3\text{H}$ coincidence data (4650 events in total) obtained in the ${}^2\text{H}({}^8\text{He}, {}^4\text{He}){}^6\text{H}$ reaction are shown in Fig. 2. The setup of experiment [2] was optimized for the ${}^7\text{H}$ search in the ${}^2\text{H}({}^8\text{He}, {}^3\text{He}){}^7\text{H}$ reaction and therefore it was not optimal for the ${}^6\text{H}$ studies. For that reason a relatively narrow center-of-mass (c.m.) angular range was available for the ${}^4\text{He}$ recoils originating from the ${}^2\text{H}({}^8\text{He}, {}^4\text{He}){}^6\text{H}$ reaction, see Fig. 2 (b). The background conditions were quite poor for these recoils because of random coincidences with alphas originating from other intense reaction channels. This background can be seen in Fig. 2 (a) as the strong population of the $\{E_T, E_{3\text{H}}\}$ plane beyond the kinematical limit for the ${}^2\text{H}({}^8\text{He}, {}^4\text{He}){}^6\text{H}$ reaction (where $E_{3\text{H}}$ is the ${}^3\text{H}$ energy in the ${}^6\text{H}$ c.m. frame). The background in the low-energy part of the MM spectrum can be drastically reduced by gating the data by the kinematically allowed range $E_{3\text{H}} < E_T/2$ in the $\{E_T, E_{3\text{H}}\}$ plane. This selection results in 3850 events, shown by red dots in Fig. 2 (b). The ${}^6\text{H}$ MM spectrum derived from these events [blue histogram in Fig. 2 (c)] shows a rise in the region beginning at $E_T = 3.0 - 3.5 \text{ MeV}$ and going up to $E_T = 6 \text{ MeV}$, where the spectrum remains flat within the energy range extending up to $E_T = 9 \text{ MeV}$. The rate of this rise, coming to the flat top, matches well the shape characteristic for relatively broad p -wave resonant states, as can be naturally expected for ${}^6\text{H}$. This rate is much faster than it can be expected for situation without resonant contributions [for example, the 4-body phase volume case is illustrated by the orange dotted curve in Fig. 2 (c)]. This specific MM spectrum shape allows us to claim that there is a resonance state, or a group of overlapping resonance states of ${}^6\text{H}$ located at MM energy $E_T \sim 6.8 \text{ MeV}$.

The 6.8 MeV peak can be made most distinct by limiting the

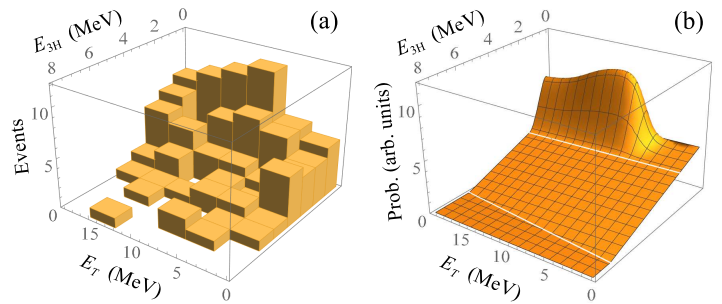


Fig. 3. (a) Empty target data in the correlation plane $\{E_T, E_{3\text{H}}\}$. (b) Empty target data fit by a smooth analytical function.

reaction c.m. range as $\theta_{\text{c.m.}} < 16^\circ$, see gray histogram in Fig. 2 (c). The MM spectra gated by some $\theta_{\text{c.m.}}$ bands with $\theta_{\text{c.m.}} > 16^\circ$ all show no resonating behavior, only monotonous growth up to $E_T \sim 20 \text{ MeV}$ [for example, see the red histogram in Fig. 2 (c)]. Partly this is due to the setup efficiency in the $E_T \sim 6.8 \text{ MeV}$ energy range, which rapidly degrades at $\theta_{\text{c.m.}} > 16^\circ$ and comes to zero at $\theta_{\text{c.m.}} \sim 22^\circ$. In contrast, the energy range $E_T \gtrsim 10 - 15 \text{ MeV}$ for $\theta_{\text{c.m.}} > 16^\circ$ is strongly boosted due to the setup geometry. This effect is well illustrated in Figs. 2 (b) and 6 (a).

The background contribution can be further reduced by taking into account the empty target data, see Fig. 3 (a). This background has two components in the $\{E_T, E_{3\text{H}}\}$ plane: the flat component, weakly depending on energy, and the “dangerous” narrow “ridge” at small $E_{3\text{H}}$ values. This background was approximated by a smooth analytical function, see Fig. 3 (b), and then a MC procedure was used to subtract it from the data. The subtraction results obtained with the empty-target data normalized to the ${}^8\text{He}$ incoming beam flux are shown in Fig. 4. It can be seen in Figs. 4 (c,d) that the subtraction procedure reduces to zero the contributions in the kinematically forbidden ranges $\varepsilon = 2E_{3\text{H}}/E_T > 1$ for the MM ranges $\{3.5, 5.5\}$ and $\{5.5, 7.5\}$. In the MM range $E_T < 3 \text{ MeV}$ the whole ${}^6\text{H}$ spectrum is effectively reduced to zero, see Fig. 4 (a). The latter observation is confirmed by the energy distribution in Fig. 4 (b): this distribution is flat and there is no considerable signature of the event concentration in the kinematically allowed range $\varepsilon < 1$.

The 6.8 MeV peak is well seen in the empty-target-corrected MM spectrum in Fig. 4 (a) with an average cross section of $\simeq 190(40) \mu\text{b/sr}$ being deduced for the c.m. angular range $5^\circ < \theta_{\text{c.m.}} < 16^\circ$. The steep rise of the spectrum at $3.0 - 3.5 \text{ MeV}$ and the broad left “wing” of the 6.8 MeV bump provide together an indication that another ${}^6\text{H}$ state can be located at about 4.5 MeV, see the discussion around Fig. 6 (c) and (d). No indication on the $2.6 - 2.9 \text{ MeV}$ state (the ${}^6\text{H}$ ground state, as suggested in Refs. [4, 5, 7]) is found. The MC simulations of our setup efficiency, see Fig. 6 (a), show that this energy range is the most favorable for resonance identification. By assuming that the *three* events, appearing at $E_T < 3.5 \text{ MeV}$, could be attributed to such a state, the cross section limit for its population is set as $d\sigma/d\Omega_{\text{c.m.}} \lesssim 3 \mu\text{b/sr}$.

Practically background-free data can be obtained additionally by taking into account the neutrons emitted in the ${}^6\text{H}$ decay. The data on ${}^4\text{He}$ - ${}^3\text{H}$ - n coincidence events (in total 130) for the ${}^2\text{H}({}^8\text{He}, {}^4\text{He}){}^6\text{H}$ reaction are shown in Fig. 5. The background level of this spectrum can be estimated as $\lesssim 3\%$ from Fig. 5 (a) and (b). There is evidence of a peak at 6.8

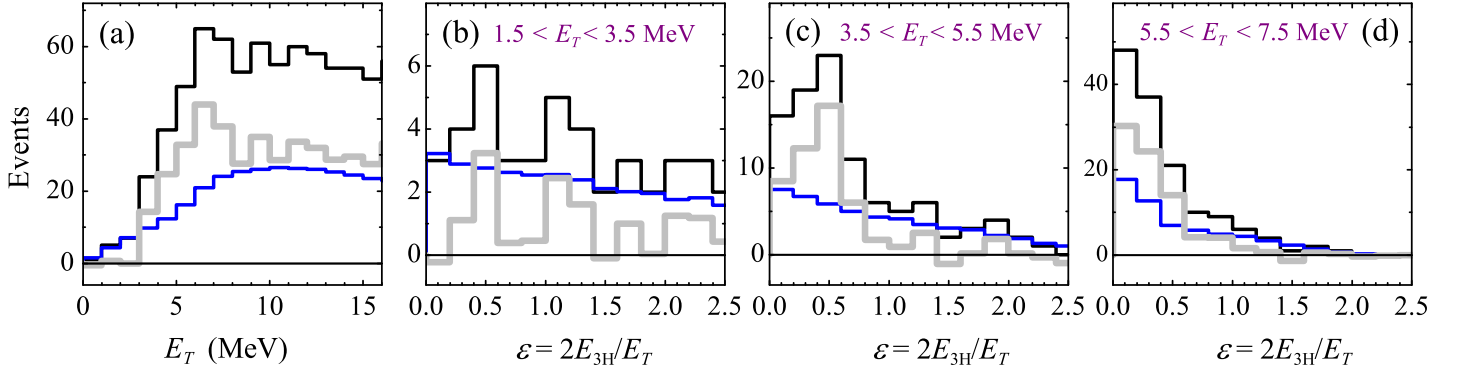


Fig. 4. Empty target background subtraction. Initial ${}^6\text{H}$ data (black histogram), scaled background (blue histogram), and corrected data (gray histogram). Panel (a) shows the ${}^6\text{H}$ MM spectrum. Panels (b), (c), and (d) show the ε distributions of the ${}^3\text{H}$ fragment in the ${}^6\text{H}$ rest frame obtained in the MM E_T ranges $\{1.5, 3.5\}$, $\{3.5, 5.5\}$, and $\{5.5, 7.5\}$ MeV, respectively.

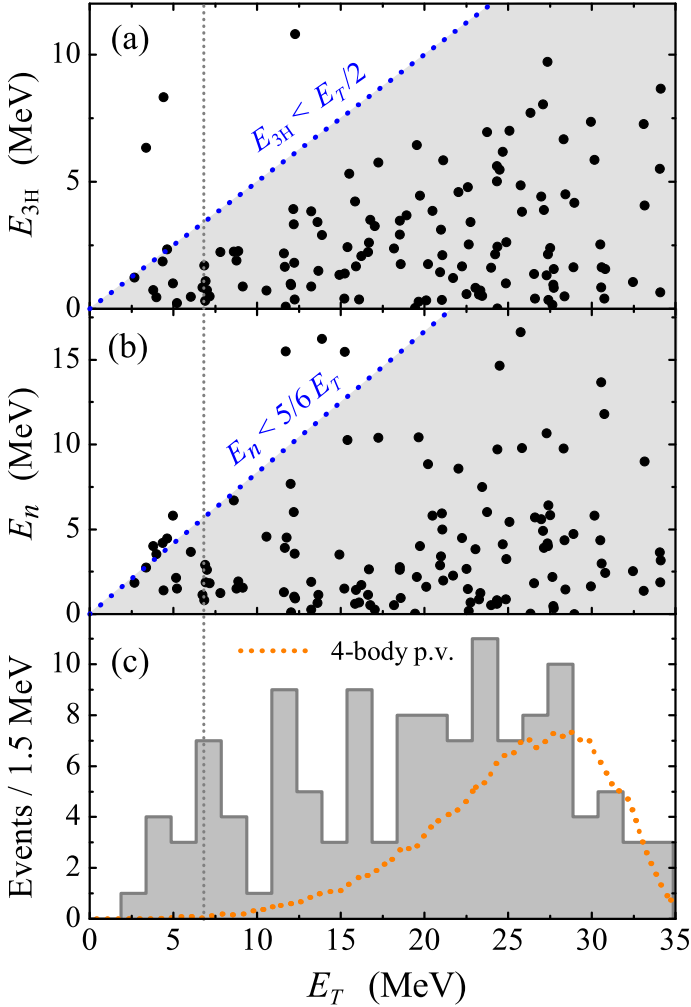


Fig. 5. The ${}^4\text{He}$ - ${}^3\text{H}$ - n coincidence events. (a) Correlation between the ${}^3\text{H}$ energy in the ${}^6\text{H}$ c.m. frame and the ${}^6\text{H}$ MM energy. (b) Correlation between the neutron energy in the ${}^6\text{H}$ c.m. frame and the ${}^6\text{H}$ MM energy. The gray triangles in (a) and (b) show the kinematically allowed regions. (c) The ${}^6\text{H}$ missing mass spectrum gated by the kinematically allowed region of panel (a). The vertical gray dotted line indicates the position of the 6.8 MeV ${}^6\text{H}$ resonant state. The orange dotted curve illustrates the 4-body phase volume $\sim E_T^{7/2}$ convoluted with the setup bias.

MeV in Fig. 5 (c), where indication on the 4.5 MeV structure can be also found.

Possible interpretations of the low-energy ${}^6\text{H}$ spectrum are

illustrated in Fig. 6. In this figure the empty-target-corrected ${}^4\text{He}$ - ${}^3\text{H}$ coincidence spectrum of Fig. 4 (a) and the ${}^4\text{He}$ - ${}^3\text{H}$ - n coincidence spectrum of Fig. 5 (c) are also corrected for the experimental efficiency by a MC procedure. The phase volume (orange dotted) curves illustrate possible profiles of nonresonant “physical backgrounds” in Fig. 6 (b) and (c). The cross section behavior at $E_T < 9$ MeV is approximated by the conventional Lorentz-like profiles

$$\frac{d\sigma}{dE_T} \sim \frac{\Gamma(E_T)}{(E_T - E_r)^2 + \Gamma(E_T)^2/4},$$

“corrected” for the energy dependence of the width defined by Eq. (3) below. The interpretation with single peak in Fig. 6 (b) seems to underestimate the spectrum in the region $E_T = 3 - 5$ MeV even for quite a broad state with $\Gamma = 3$ MeV. For the $E_T = 6.8$ MeV resonance of a smaller width (e.g. $\Gamma = 1.5$ MeV) the interpretation with two states, illustrated in Fig. 6 (c), is preferable. The $E_T = 4.5$ MeV peak can be interpreted as the lowest ${}^6\text{H}$ resonant state energy, which can be consistent with our data. However, one should keep in mind that more than two overlapping ${}^6\text{H}$ states may actually be expected in this energy range, see Section 5. Therefore, “two-state situation” in reality could mean “more than one state”.

4. True and sequential decay of ${}^6\text{H}$

The simplest realistic idea about the character of the 4-body decay is based on the phase volume (p.v.) approximation. The phase space dV_4 of the 4-particle system can be defined by the three energies $E_i = \varepsilon_i E_T$ corresponding to the three Jacobi vectors in momentum space

$$dV_4 \sim E_T^{9/2} \delta(E_T - \sum_i \varepsilon_i E_T) \sqrt{\varepsilon_1 \varepsilon_2 \varepsilon_3} d\varepsilon_1 d\varepsilon_2 d\varepsilon_3. \quad (1)$$

The one-dimensional phase-volume energy distribution can be obtained by integrating the phase space (1) over the two ε variables

$$dV_4/d\varepsilon \sim E_T^{7/2} \sqrt{\varepsilon(1-\varepsilon)^4}. \quad (2)$$

This expression for the energy distribution is evidently the same for any of the three Jacobi vectors. Therefore, it defines the single-particle energy distributions both for ${}^3\text{H}$ and n fragments emitted in the ${}^6\text{H}$ decay.

For the sequential decay of ${}^6\text{H}$ via the ${}^5\text{H}$ g.s. we employ the generalization of the R-matrix-type expression, which was

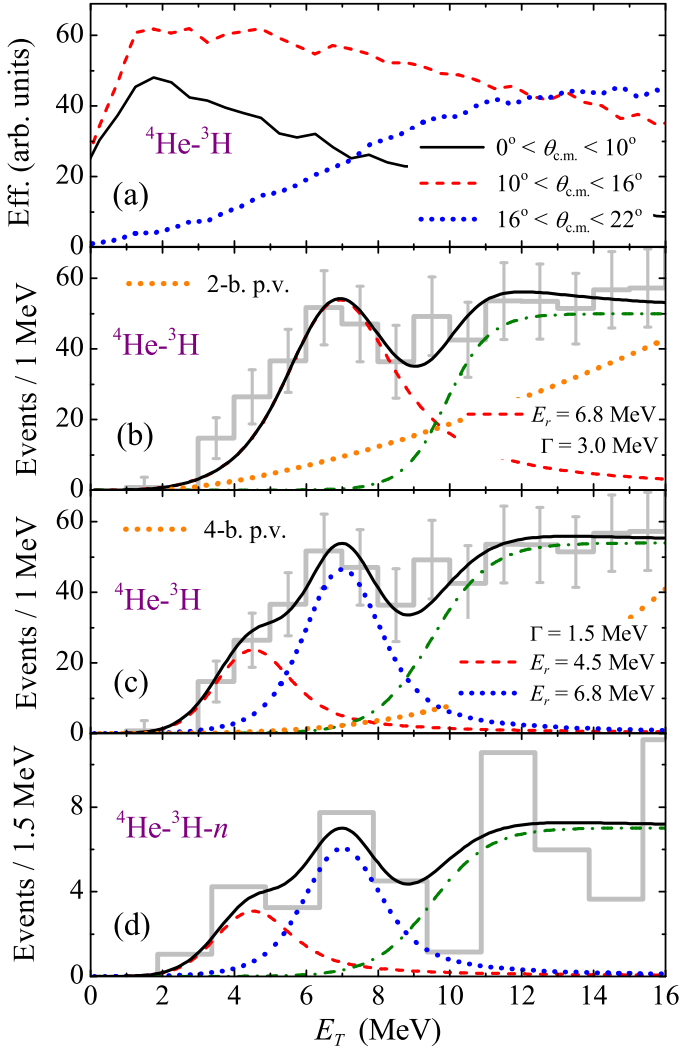


Fig. 6. (a) Efficiency of the ${}^4\text{He}-{}^3\text{H}$ coincidence registration in different $\theta_{\text{c.m.}}$ ranges. Possible interpretations of the ${}^6\text{H}$ spectrum with one broad (b) or two relatively narrow states (c) and (d). The gray histograms in (b) and (c) show the efficiency-corrected ${}^4\text{He}-{}^3\text{H}$ coincidence data based on Fig. 4 (a). The gray histogram in (d) shows the efficiency-corrected ${}^4\text{He}-{}^3\text{H}-n$ coincidence data based on Fig. 5 (c). The red dashed and blue dotted curves correspond to the possible contributions of the low-energy ${}^6\text{H}$ states, the green dash-dotted curve is an option for the physical background approximated by the Fermi-type profile. The 2-body phase volume $\sim (E_T - E_{5\text{H}}^{(R)})^{3/2}$ for the p -wave ${}^5\text{H}(\text{g.s.})+n$ channel and the 4-body phase volume $\sim E_T^{7/2}$ and are shown by the orange dotted lines in (b) and (c), respectively.

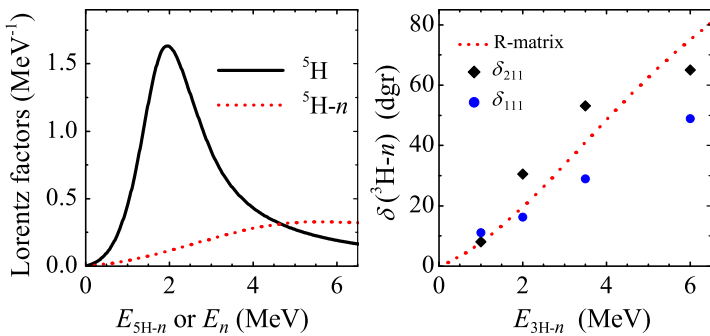


Fig. 7. (a) The Lorentz profiles, as used in Eq. (3), for the ${}^5\text{H}(\text{g.s.})$ subsystem and for the ${}^5\text{H}-n$ relative motion. (b) Phase shifts, corresponding to the ${}^5\text{H}-n$ profile in panel (a), are compared with the experimental phase shifts of the lower spin-doublet states in ${}^4\text{H}$ with the $\{j, l, s\}$ sets $\{1, 1, 1\}$ and $\{2, 1, 1\}$.

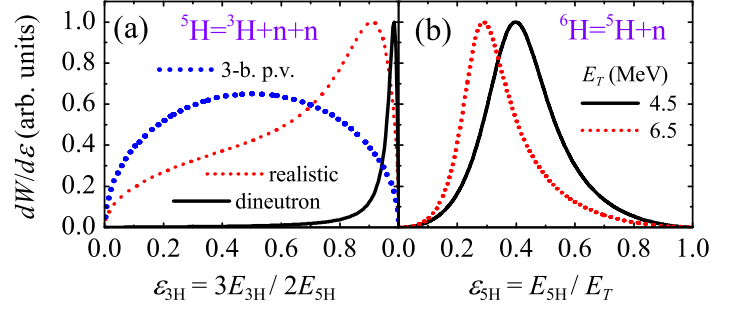


Fig. 8. The ε energy distributions. (a) For the ${}^5\text{H}(\text{g.s.})$ decay, between the ${}^3\text{H}$ and $2n$ for different model assumptions about the decay dynamics. (b) For the ${}^6\text{H}(\text{g.s.})$ decay, between the ${}^5\text{H}(\text{g.s.})$ and neutron.

previously actively used for the two-nucleon emission estimates in Refs. [14, 15, 16, 17, 18]:

$$\begin{aligned} \frac{\Gamma(E_T)}{d\varepsilon_{5\text{H}}} &= \frac{E_T \langle V_3 \rangle^2}{2\pi} \frac{\Gamma_{5\text{H}-n}(E_{5\text{H}-n})}{(E_{5\text{H}-n} - E_{5\text{H}-n}^{(R)})^2 - \Gamma_{5\text{H}-n}^2(E_{5\text{H}-n})/4} \\ &\times \frac{\Gamma_{5\text{H}}(E_{5\text{H}})}{(E_{5\text{H}} - E_{5\text{H}}^{(R)})^2 - \Gamma_{5\text{H}}^2(E_{5\text{H}})/4}, \\ \langle V_3 \rangle^2 &= (E_T - E_{5\text{H}}^{(R)} - E_n^{(R)})^2 + \Gamma^2(E_T)/4, \\ E_{5\text{H}} &= \varepsilon_{5\text{H}} E_T, \quad E_{5\text{H}-n} = (1 - \varepsilon_{5\text{H}}) E_T, \end{aligned} \quad (3)$$

where the Γ value in $\langle V_3 \rangle^2$ is defined in a self-consistent way. The $\Gamma_{5\text{H}}$ width dependence can be parameterized as

$$\Gamma_{5\text{H}}(E_{5\text{H}}) = C_{5\text{H}} E_{5\text{H}}^2, \quad C_{5\text{H}} = 0.5 \text{ MeV}^{-1}. \quad (4)$$

For $E_{5\text{H}}^{(R)} = 1.8$ MeV this results in $\Gamma_{5\text{H}} = 1.62$ MeV, which is consistent with the data [8, 10]. The neutron width can be defined by the standard R-matrix expression

$$\Gamma_{5\text{H}-n}(E_{5\text{H}-n}) = 2 \frac{\theta^2}{2Mr_c^2} P_{l=1}(E_{5\text{H}-n}, r_c), \quad (5)$$

where P_l is penetrability as a function of the decay energy $E_{5\text{H}-n}$ in the ${}^5\text{H}+n$ channel and its “channel radius” r_c . The Lorentz-type profiles used in Eq. (3) for the ${}^6\text{H}$ estimates are shown in Fig. 7 (a). They correspond to the following parameters: $E_{5\text{H}} = 2.25$ MeV, $E_{5\text{H}-n}^{(R)} = 7$ MeV, $r_c = 4$ fm, and $\theta^2 = 2$. The phase shift in the ${}^3\text{H}-n$ channel, which can be associated with Γ_n in Eq. (5), is shown in Fig. 7 (b): this can be seen as an average of the two lowest states of ${}^4\text{H}$. The energy distribution between the ${}^5\text{H}(\text{g.s.})$ and neutron, calculated by the Eq. (3), is shown in Fig. 8 (b) for two ${}^6\text{H}$ decay energies. The ${}^6\text{H}$ decay widths, estimated by Eq. (3), for the states with $E_T = 4.5$ and 6.8 MeV vary from 0.5 to 2 MeV: they are quite sensitive to the parameterization detail of Eqs. (4) and (5). The ${}^6\text{H}$ g.s. may have quite low spectroscopic factor for the $n+{}^5\text{H}(\text{g.s.})$ configuration spectroscopy in analogy with the ${}^7\text{He}$ g.s. situation, where respective neutron spectroscopic factors $0.3-0.6$ are typically derived or predicted (e.g. [19, 20], and Refs. therein). Therefore, one cannot exclude the widths of the ${}^6\text{H}$ g.s. being as small as few hundreds of keV.

In order to calculate the fragment distributions in the decay of ${}^6\text{H}$, another required input is the energy distribution ${}^3\text{H}+n+n$ inside the ${}^5\text{H}$ subsystem. Here we employ the following three qualitatively different model distributions: (i) “3-b. p.v.” — three-body phase volume assumption about the decay of the ${}^5\text{H}$ g.s. (the standard uncorrelated assumption),

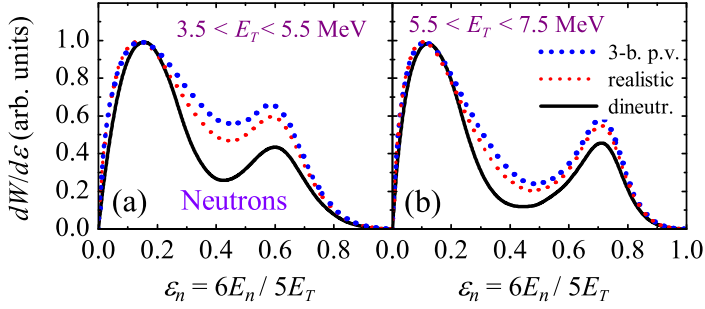


Fig. 9. The calculated ε energy distributions of neutrons emitted from the ${}^6\text{H}$ states at $E_T = 4.5$ MeV (a) and $E_T = 6.8$ MeV (b). The black solid, red dashed, and blue dotted curves correspond to the “dineutron”, “realistic”, and 3-body phase volume models of the ${}^5\text{H}$ g.s. decay, respectively.

(ii) “realistic” — the ${}^5\text{H}$ g.s. energy distribution inspired by the experimental data [10], and (iii) “dineutron” — the highly correlated dineutron decay of the ${}^5\text{H}$ ground state. These cases are illustrated in Fig. 8 (a). It should be understood what this “inspired by experiment” assumption means: the energy distribution for ${}^5\text{H}$ was reconstructed in [10] in the energy range around the g.s. position (see Figs. 10 and 11 in [10]). However, it is demonstrated in [10] that in the ${}^5\text{H}$ g.s. energy region ($E_T \sim 1.8$ MeV) the contribution of the broad $5/2^+ - 3/2^+$ doublet of excited ${}^5\text{H}$ states (located around $E_T \sim 5$ MeV) is large or even dominant. For that reason we can only guess or try to predict theoretically [21, 22, 23] what is the actual ${}^5\text{H}$ g.s. decay energy distribution.

By using the inputs from Figs. 7 and 8 we obtain the energy distributions of the neutrons and ${}^3\text{H}$ fragments in the ${}^6\text{H}$ rest frame, see Fig. 9 and Fig. 10, respectively. The estimated neutron distributions all have a pronounced bimodal character connected with the assumed sequential ${}^6\text{H} \rightarrow {}^5\text{H}(\text{g.s.}) + n \rightarrow {}^3\text{H} + 3n$ mechanism of the decay. Unfortunately, the single-neutron distribution is relatively weakly sensitive to the decay mechanism of ${}^5\text{H}$, and the energy resolution of the neutron spectrum in Fig. 5 is not sufficient to make practical use of this information. In contrast, the ${}^3\text{H}$ energy distribution demonstrates strong sensitivity to the correlations in the ${}^5\text{H}$ intermediate system.

To make the above considerations quantitative, the ${}^3\text{H}$ energy distributions of Figs. 10 (a,b) were used in MC simulations, which allowed us to take into account the bias of our experimental setup. The resulting distributions are shown in Figs. 10 (c,d), and the numerical information about the ${}^3\text{H}$ energy distributions is provided in Table 1.

The experimental energy distributions for the ${}^3\text{H}$ fragment in the ${}^6\text{H}$ c.m. system are shown in Fig. 10 (e,f) for the ${}^4\text{He}-{}^3\text{H}$ and ${}^4\text{He}-{}^3\text{H}-n$ coincidence events. These distributions in the energy ranges $E_T = 3.5 - 5.5$ MeV and $E_T = 5.5 - 7.5$ MeV are consistent with each other within the available statistics. It can be understood from Fig. 10 and Table 1 that the preferable interpretation of the data suggests the extremely correlated emission of two neutrons from the ${}^5\text{H}(\text{g.s.})$ intermediate system.

5. Discussion

Let us consider the energy level evolution from ${}^5\text{He}$ (with the assumed configuration of one neutron particle in the $p_{3/2}$ subshell) to ${}^7\text{He}$ (one neutron hole in the $p_{3/2}$ subshell), see

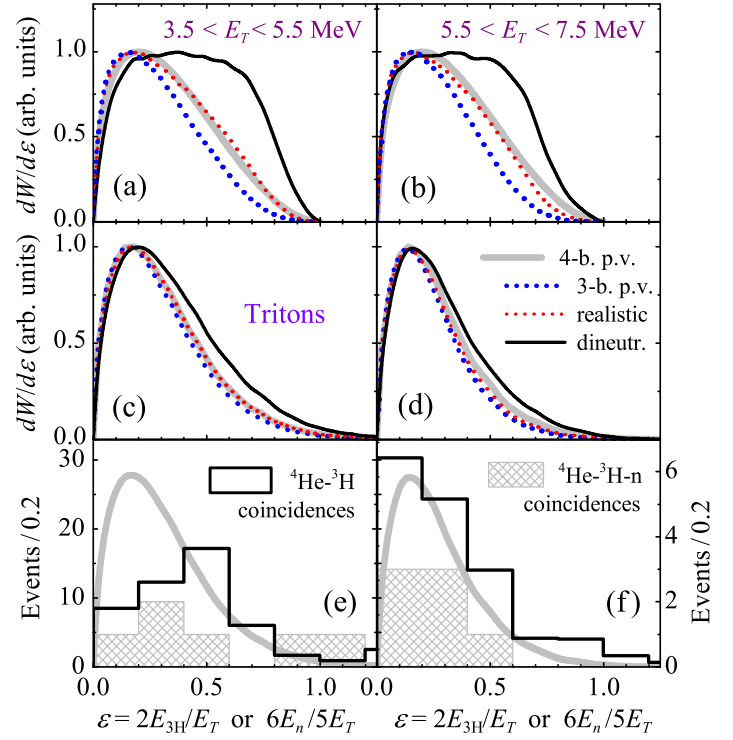


Fig. 10. The ε energy distributions of ${}^3\text{H}$ fragments emitted from the ${}^6\text{H}$ states at $E_T = 4.5$ MeV (a,c,e) and $E_T = 6.8$ MeV (b,d,f). The black solid, red dashed, and blue dotted curves correspond to the “dineutron”, “realistic”, and 3-body phase volume models of the ${}^5\text{H}$ g.s. decay, respectively. The thick gray curve shows the 4-body phase volume distribution Eq. (2). Panels (a,b) show the initial theoretical distributions, while in panels (c,d) the experimental setup bias is taken into account via MC procedure. Panels (e,f) show the experimental ε energy distributions for the ${}^3\text{H}$ fragment in the E_T energy ranges $\{3.5, 5.5\}$ and $\{5.5, 7.5\}$ MeV. The black histograms show the distributions obtained from the ${}^4\text{He}-{}^3\text{H}$ coincidence data (left axis). The gray hatched histograms show the distributions obtained from the ${}^4\text{He}-{}^3\text{H}-n$ coincidence data (right axis). The MC 4-body phase volume distributions are shown by the thick gray curves.

Figure 11. The $3/2^-$ ground state of ${}^7\text{He}$ becomes somewhat more bound, than that in ${}^5\text{He}$. The experimental status of the $1/2^-$ state in ${}^7\text{He}$ is not well established, however, it seems clear that it has higher excitation energy than in ${}^5\text{He}$. Moreover, it is very likely that there is the $5/2^-$ state in ${}^7\text{He}$, built on the 2^+ excitation of ${}^6\text{He}$ [24, 25], which, evidently, has no counterpart in ${}^5\text{He}$.

If we consider evolution from ${}^5\text{He}$ to ${}^4\text{H}$, then the $\{3/2^-, 1/2^-\}$ spin-orbit doublet is replaced by a quadruplet $\{2^-, 1^-, 1^-, 0^-\}$ of states obtained by a split due to the ${}^3\text{H}$ spin. If we extend the ${}^5\text{He}-{}^7\text{He}$ analogy of Fig. 11 to the ${}^6\text{H}$ states, then two effects are expected.

(i) Following the ${}^7\text{He}$ vs. ${}^5\text{He}$ analogy, we expect that the ${}^6\text{H}$ g.s. is more bound than the ${}^4\text{H}$ ground state. This assumption is true if the 4.5 MeV state really exists in ${}^6\text{H}$.

(ii) In the range $4 < E_T < 9$ MeV we expect *six* states of ${}^6\text{H}$. So, it is very likely that the broad 6.8 MeV structure is actually a superposition of several overlapping states, which are populated in unknown proportions and could not be resolved in the inclusive (no correlation) experiment. It still makes sense to isolate the 4.5 MeV state specially, as the lowest energy resonance, which is allowed by our data and, thus, a candidate to represent ${}^6\text{H}$ ground state.

As we have mentioned in Introduction, the ${}^6\text{H}$ g.s. position was suggested to be at $E_T = 2.6 - 2.9$ MeV in Refs. [4, 5, 7]. However, now the g.s. energies are known for ${}^5\text{H}$ (at ~ 1.8 MeV

Table 1

Mean values of the ε distributions in the two E_T energy ranges. The “th.” columns show the theoretical results and “bias” columns give the corresponding values corrected for the experimental bias via the MC procedure. The “4-body p.v.” is the four-body phase volume approximation of the true $3n$ emission from ${}^6\text{H}$ by Eq. (2). Models for the sequential ${}^6\text{H} \rightarrow {}^5\text{H}(\text{g.s.}) + n \rightarrow {}^3\text{H} + 3n$ decay: “3-body p.v.” — the uncorrelated three-body phase volume decay of the ${}^5\text{H}$ g.s., “realistic” — the experiment-inspired distribution for the ${}^5\text{H}$ g.s., “dineutron” — the highly correlated dineutron decay of the ${}^5\text{H}$ ground state. The column “experiment” shows the data from Figs. 5 and 10. The experimental errors are calculated by the MC procedure based on the available experimental statistics in each case.

Models: ranges (MeV)	4-body p.v.		3-body p.v.		realistic		dineutron		experiment	
	th.	bias	th.	bias	th.	bias	th.	bias	${}^4\text{He}-{}^3\text{H}$	${}^4\text{He}-{}^3\text{H}-n$
$3.5 < E_T < 5.5$	1/3	0.30	0.29	0.28	0.33	0.30	0.43	0.39	0.42(3)	0.49(7)
$5.5 < E_T < 7.5$	1/3	0.28	0.27	0.24	0.31	0.26	0.39	0.33	0.33(2)	0.24(8)

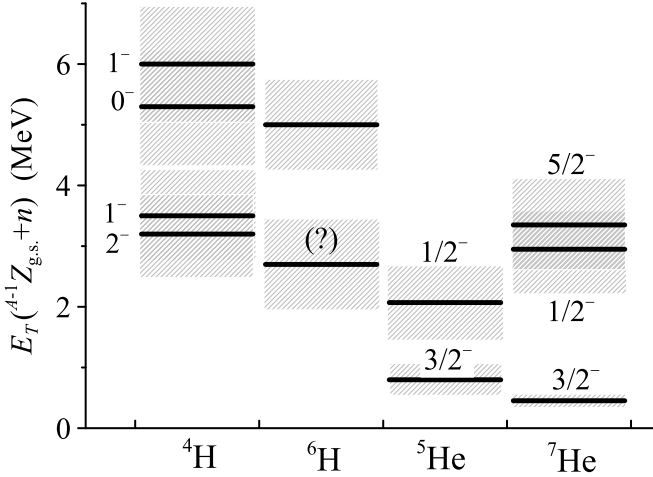


Fig. 11. Evolution of the level scheme of the ${}^5\text{He}$ - ${}^4\text{H}$ pair (one neutron particle in the $p_{3/2}$ subshell) and the ${}^7\text{He}$ - ${}^6\text{H}$ pair (one neutron hole in the $p_{3/2}$ subshell). The energies are calculated relatively to the one-neutron separation threshold (the ${}^5\text{H}$ g.s. is assumed to be 1.8 MeV above the two-neutron separation threshold [8, 10]).

[8, 10]; the 2.4(3) MeV value from [26] is practically consistent with this value) and ${}^7\text{H}$ (at ~ 2.2 MeV [2]; we regard the $\sim 0.3 - 1$ MeV value from [7] as much less reliable). Based on these values, the energy reported in [4, 5, 7] for the ${}^6\text{H}$ ground state, would mean the lack of the neutron pairing effect in the even-neutron nucleus ${}^7\text{H}$ (experimental pairing energy appears to be $\sim 0.7 - 1$ MeV compared with ~ 3 MeV expected from analogy with the ${}^7\text{He}$ - ${}^8\text{He}$ pair). Hence, we conclude that the results reported in Refs. [4, 5, 7] are not compatible with the standard pairing assumption. The ${}^6\text{H}$ ground state suggested in this work at $E_T = 4.5$ MeV precisely fits the pairing energy systematics.

The search for ${}^6\text{H}$ in the ${}^6\text{Li}(\pi^-, \pi^+)$ reaction provided no g.s. identification. However, the peculiar behavior of the low-energy ${}^6\text{H}$ missing mass spectrum was explained in [27] as due to presence of strongly correlated $2n$ configuration in the ${}^6\text{H}$ continuum ${}^3\text{H} + n + 2n$. This idea is in agreement with the observations of correlations made in [10] and in this work.

6. Conclusions

The ${}^6\text{H}$ spectrum was studied in this work in the ${}^2\text{H}({}^8\text{He}, {}^4\text{He}){}^6\text{H}$ transfer reaction. The peak in the ${}^6\text{H}$ MM spectrum at $E_T = 6.8(5)$ MeV is reliably identified in the data with the resonant cross-section $d\sigma/d\Omega_{\text{c.m.}} \simeq 190(40) \mu\text{b/sr}$ in the $5^\circ < \theta_{\text{c.m.}} < 16^\circ$ angular range. Observation of such

a peak is consistent with the observations of Ref. [6]. This could be a state or a set of broad overlapping p -wave states, as expected from analogy with the known ${}^4\text{H}$ spectrum. We have found *no evidence* of the $\sim 2.6 - 2.9$ MeV state in ${}^6\text{H}$, which was reported in the pioneering work [4] and has got support in [5, 7]. The cross section limit $d\sigma/d\Omega_{\text{c.m.}} \lesssim 3 \mu\text{b/sr}$ is set for the population of possible states with $E_T < 3.5$ MeV. Also the existence of the ${}^6\text{H}$ g.s. at $\sim 2.6 - 2.9$ MeV is hardly consistent, due to the pairing energy argument, with the observation of the ${}^7\text{H}$ g.s. at 2.2(5) MeV [2]. The interpretation of our data also allows for $E_T = 4.5(3)$ MeV state, which should be understood as the lowest-energy ${}^6\text{H}$ resonant state admissible by our data. According to systematics arguments, such a state is a good candidate to be the ${}^6\text{H}$ ground state.

The momentum distribution of the ${}^3\text{H}$ decay fragments was reconstructed in the ${}^6\text{H}$ rest frame. In this work the theoretical studies of the four-body sequential ${}^6\text{H} \rightarrow {}^5\text{H}(\text{g.s.}) + n \rightarrow {}^3\text{H} + 3n$ decays were performed for the first time. Within the assumption of the ${}^6\text{H}$ sequential decay we have found that our data provide evidence that an extremely strong “dineutron-type” correlation is realized in the decay of the ${}^5\text{H}$ ground state. More accurate measurements are needed for more solid conclusions. However, a potentially powerful approach for extracting information about the nuclear decay dynamics is already illustrated in our work.

Acknowledgments. — This work was partly supported by the Russian Science Foundation grant No. 17-12-01367. The authors are grateful to Prof. M.S. Golovkov for help in the work and useful remarks. We acknowledge the interest and support of this activity from Profs. Yu.Ts. Oganessian and S.N. Dmitriev.

REFERENCES

1. A. A. Bezbakh, V. Chudoba, S. A. Krupko, S. G. Belogurov, D. Biare, A. S. Fomichev, E. M. Gazeeva, A. V. Gorshkov, L. V. Grigorenko, G. Kaminski, O. A. Kiselev, D. A. Kostyleva, M. Y. Kozlov, B. Mauryey, I. Mukha, I. A. Muzalevskii, E. Y. Nikolskii, Y. L. Parfenova, W. Piatek, A. M. Quynh, V. N. Schetinina, A. Serikov, S. I. Sidorchuk, P. G. Sharov, R. S. Slepnev, S. V. Stepantsov, A. Swiercz, P. Szymkiewicz, G. M. Ter-Akopian, R. Wolski, B. Zalewski, M. V. Zhukov, Phys. Rev. Lett. 124 (2020) 022502.
2. I. A. Muzalevskii, A. A. Bezbakh, E. Y. Nikolskii, V. Chudoba, S. A. Krupko, S. G. Belogurov, D. Biare, A. S. Fomichev, E. M. Gazeeva, A. V. Gorshkov, L. V. Grigorenko, G. Kaminski, O. Kiselev, D. A. Kostyleva, M. Y. Kozlov, B. Mauryey, I. Mukha, Y. L. Parfenova, W. Pi-

- atek, A. M. Quynh, V. N. Schetinin, A. Serikov, S. I. Sidorchuk, P. G. Sharov, N. B. Shulgina, R. S. Slepnev, S. V. Stepantsov, A. Swiercz, P. Szymkiewicz, G. M. Ter-Akopian, R. Wolski, B. Zalewski, M. V. Zhukov, *Phys. Rev. C* 103 (2021) 044313.
3. L. Grigorenko, P. Sharov, R. Wolski, I. Muzalevskii, A. Bezbakh, V. Chudoba, A. Fomichev, I. Mukha, E. Y. Nikolskii, G. M. Ter-Akopian, M. V. Zhukov, (to be submitted).
4. D. Aleksandrov, E. Ganza, Yu.A.Glukhov, B.G.Novatsky, A.A.Ogloblin, D.N.Stepanov, *Yad. Fiz.* 39 (1984) 513.
5. A. Belozorov, C. Borcea, Z. Dlouhy, A. Kalinin, R. Kalpakchieva, N. H. Chau, Y. Oganessian, Y. Penionzhkevich, *Nuclear Physics A* 460 (1986) 352–360.
6. Y. Gurov, B. Chernyshev, S. Isakov, V. S. Karpukhin, S. Lapushkin, I. V. Laukhin, V. A. Pechkurov, N. O. Poroshin, V. Sandukovsky, *The European Physical Journal A* 32 (3) (2007) 261–266.
7. M. Caamaño, D. Cortina-Gil, W. Mittig, H. Savajols, M. Chartier, C. E. Demonchy, B. Fernández, M. B. G. Hornillos, A. Gillibert, B. Jurado, O. Kiselev, R. Lemmon, A. Obertelli, F. Rejmund, M. Rejmund, P. Roussel-Chomaz, R. Wolski, *Phys. Rev. C* 78 (2008) 044001.
8. A. A. Korshennikov, M. S. Golovkov, I. Tanihata, A. M. Rodin, A. S. Fomichev, S. I. Sidorchuk, S. V. Stepantsov, M. L. Chelnokov, V. A. Gorshkov, D. D. Bogdanov, R. Wolski, G. M. Ter-Akopian, Y. T. Oganessian, W. Mittig, P. Roussel-Chomaz, H. Savajols, E. A. Kuzmin, E. Y. Nikolskii, A. A. Ogloblin, *Phys. Rev. Lett.* 87 (2001) 092501.
9. M. S. Golovkov, L. V. Grigorenko, A. S. Fomichev, S. A. Krupko, Y. T. Oganessian, A. M. Rodin, S. I. Sidorchuk, R. S. Slepnev, S. V. Stepantsov, G. M. Ter-Akopian, R. Wolski, M. G. Itkis, A. A. Bogatchev, N. A. Kondratiev, E. M. Kozulin, A. A. Korshennikov, E. Y. Nikolskii, P. Roussel-Chomaz, W. Mittig, R. Palit, V. Bouchat, V. Kinnard, T. Materna, F. Hanappe, O. Dorvaux, L. Stuttgé, C. Angulo, V. Lapoux, R. Raabe, L. Nalpas, A. A. Yukhimchuk, V. V. Perevozchikov, Y. I. Vinogradov, S. K. Grishechkin, S. V. Zlatoustovskiy, *Phys. Rev. Lett.* 93 (2004) 262501.
10. M. S. Golovkov, L. V. Grigorenko, A. S. Fomichev, S. A. Krupko, Y. T. Oganessian, A. M. Rodin, S. I. Sidorchuk, R. S. Slepnev, S. V. Stepantsov, G. M. Ter-Akopian, R. Wolski, M. G. Itkis, A. S. Denikin, A. A. Bogatchev, N. A. Kondratiev, E. M. Kozulin, A. A. Korshennikov, E. Y. Nikolskii, P. Roussel-Chomaz, W. Mittig, R. Palit, V. Bouchat, V. Kinnard, T. Materna, F. Hanappe, O. Dorvaux, L. Stuttgé, C. Angulo, V. Lapoux, R. Raabe, L. Nalpas, A. A. Yukhimchuk, V. V. Perevozchikov, Y. I. Vinogradov, S. K. Grishechkin, S. V. Zlatoustovskiy, *Phys. Rev. C* 72 (2005) 064612.
11. I. Muzalevskii, V. Chudoba, S. Belogurov, D. B. A.A. Bezbakh, A. Fomichev, S. Krupko, E.M.Gazeeva, M.S.Golovkov, A.V.Gorshkov, L.V.Grigorenko, G.Kaminski, O.Kiselev, D.A.Kostyleva, M.Yu.Kozlov, B.Mauey, I.Mukha, E.Yu.Nikolskii, Yu.L.Parfenova, W.Piatek, A.M.Quynh, V.N.Schetinin, A.Serikov, S.I.Sidorchuk, P.G.Sharov, R.S.Slepnev, S.V.Stepantsov, A.Swiercz, P.Szymkiewicz, G.M.Ter-Akopian, R.Wolski, B.Zalewski, *Bulletin of the Russian Academy of Sciences: Physics* 84 (2020) 500–504.
12. A. S. Fomichev, L. V. Grigorenko, S. A. Krupko, S. V. Stepantsov, G. M. Ter-Akopian, *The European Physical Journal A* 54 (6) (2018) 97.
13. A. A. Bezbakh, S. G. Belogurov, R. Wolski, E. M. Gazeeva, M. S. Golovkov, A. V. Gorshkov, G. Kaminski, M. Y. Kozlov, S. A. Krupko, I. A. Muzalevsky, E. Y. Nikolskii, E. V. Ovcharenko, R. S. Slepnev, G. M. Ter-Akopian, A. S. Fomichev, P. G. S. V. Chudoba, V. N. Schetinin, *Instruments and Experimental Techniques* 61 (2018) 631–638.
14. L. V. Grigorenko, M. V. Zhukov, *Phys. Rev. C* 76 (2007) 014009.
15. L. V. Grigorenko, T. D. Wiser, K. Mercurio, R. J. Charity, R. Shane, L. G. Sobotka, J. M. Elson, A. H. Wuosmaa, A. Banu, M. McCleskey, L. Trache, R. E. Tribble, M. V. Zhukov, *Phys. Rev. C* 80 (2009) 034602.
16. E. Olsen, M. Pfützner, N. Birge, M. Brown, W. Nazarewicz, A. Perhac, *Phys. Rev. Lett.* 110 (2013) 222501.
17. K. W. Brown, R. J. Charity, L. G. Sobotka, L. V. Grigorenko, T. A. Golubkova, S. Bedoor, W. W. Buhro, Z. Chajecski, J. M. Elson, W. G. Lynch, J. Manfredi, D. G. McNeel, W. Reviol, R. Shane, R. H. Showalter, M. B. Tsang, J. R. Winkelbauer, A. H. Wuosmaa, *Phys. Rev. C* 92 (2015) 034329.
18. L. V. Grigorenko, M. V. Zhukov, *Phys. Rev. C* 91 (2015) 064617.
19. F. Renzi, R. Raabe, G. Randisi, D. Smirnov, C. Angulo, J. Cabrera, E. Casarejos, T. Keutgen, A. Ninane, J. L. Charvet, A. Gillibert, V. Lapoux, L. Nalpas, A. Obertelli, F. Skaza, J. L. Sida, N. A. Orr, S. I. Sidorchuk, R. Wolski, M. J. G. Borge, D. Escrig, *Phys. Rev. C* 94 (2016) 024619.
20. H. T. Fortune, *Eur. Phys. J. A* 54 (2018) 51.
21. N. B. Shul'gina, B. V. Danilin, L. V. Grigorenko, M. V. Zhukov, J. M. Bang, *Phys. Rev. C* 62 (2000) 014312.
22. L. V. Grigorenko, N. K. Timofeyuk, M. V. Zhukov, *Eur. Phys. J. A* 19 (2004) 187.
23. L. V. Grigorenko, *Eur. Phys. J. A* 20 (2004) 419.
24. A. A. Korshennikov, M. S. Golovkov, A. Ozawa, E. A. Kuzmin, E. Y. Nikolskii, K. Yoshida, B. G. Novatskii, A. A. Ogloblin, I. Tanihata, Z. Fulop, K. Kusaka, K. Morimoto, H. Otsu, H. Petrascu, F. Tokanai, *Phys. Rev. Lett.* 82 (1999) 3581–3584.
25. A. H. Wuosmaa, J. P. Schiffer, K. E. Rehm, J. P. Greene, D. J. Henderson, R. V. F. Janssens, C. L. Jiang, L. Jisonna, J. C. Lighthall, S. T. Marley, E. F. Moore, R. C. Pardo, N. Patel, M. Paul, D. Peterson, S. C. Pieper, G. Savard, R. E. Segel, R. H. Siemssen, X. D. Tang, R. B. Wiringa, *Phys. Rev. C* 78 (2008) 041302.
26. A. H. Wuosmaa, S. Bedoor, K. W. Brown, W. W. Buhro, Z. Chajecski, R. J. Charity, W. G. Lynch, J. Manfredi, S. T. Marley, D. G. McNeel, A. S. Newton, D. V. Shetty, R. H. Showalter, L. G. Sobotka, M. B. Tsang, J. R. Winkelbauer, R. B. Wiringa, *Phys. Rev. C* 95 (2017) 014310.
27. K. K. Seth, B. Parker, *Phys. Rev. Lett.* 66 (1991) 2448–2451.